

# Evaluation of Data Pretreatment and Model Building Methods for the Determination of Glucose from Near-Infrared Single-Beam Spectra

QING DING, GARY W. SMALL,\* and MARK A. ARNOLD

*Center for Intelligent Chemical Instrumentation, Department of Chemistry and Biochemistry, Ohio University, Athens, Ohio 45701 (Q.D., G.W.S.); and Department of Chemistry, Iowa Advanced Technology Laboratories, University of Iowa, Iowa City, Iowa 52242 (M.A.A.)*

Near-infrared single-beam spectra are used to build partial least-squares (PLS) calibration models for the determination of glucose in biological matrices. Two different data sets of the same sample constituents are used in this investigation. The glucose samples consist of an aqueous matrix of varied concentrations of bovine serum albumin (BSA) and triacetin. The BSA and triacetin are models for blood proteins and triglycerides, respectively. Due to the effects of intensity variation in the single-beam spectra, calibration models obtained with unprocessed spectra are not as good as those computed with the corresponding spectra in absorbance units. When this intensity variation is reduced through the use of multiplicative signal correction (MSC), a spectral normalization method, or a logarithmic transform, the resulting models are as good as or better than those obtained in the analysis of absorbance spectra. An attempt is made to model the nonlinear relationship between single-beam spectral intensities and glucose concentrations by use of stepwise quadratic PLS (QPLS) models. The QPLS models are found to perform better than linear PLS models in some cases (e.g., with MSC-corrected single-beam spectra). The effect of digital filtering on the calibration models computed with single-beam spectra is also studied. The results obtained with and without filtering are found to be similar in terms of model performance, but the models based on filtered single-beam intensities require fewer latent variables and perform more consistently as a group. A final test is performed to compare the robustness of calibration models computed with single-beam spectra to those based on absorbance spectra. When applied to spectra that lie outside the time span of the calibration data, the models based on single-beam spectra are still competitive with those computed with absorbance spectra.

Index Headings: Near-infrared; Glucose; Single-beam spectra; Multivariate calibration; Partial least-squares.

## INTRODUCTION

The motivation for noninvasive blood glucose measurements arises from the need of diabetic patients to maintain strict control of their glucose levels and the resulting requirement for frequent glucose monitoring. Among the approaches studied for potential application to this measurement, near-infrared (near-IR) spectroscopy has been investigated most.<sup>1-4</sup> To achieve the ultimate goal of developing a noninvasive glucose sensor, work in our laboratories has focused on near-IR transmission measurements of samples in which clinically relevant glucose levels are combined with background matrices of increasing complexity.<sup>5-13</sup>

Most previous studies have been based on the analysis of near-IR spectra in absorbance units. This is the con-

ventional approach used in spectroscopic analyses based on the Beer-Lambert law. The spectra used are obtained by ratioing the single-beam spectra of glucose samples to representative background single-beam spectra. The use of ratioed spectra helps to remove variation in the sample spectrum that is unrelated to the spectral variation arising from changes in the concentrations of the matrix constituents.

Unfortunately, the collection of a glucose-depleted background spectrum for use in the context of a noninvasive glucose measurement is impossible. This consideration has motivated us to investigate the feasibility of building multivariate calibration models based on the direct use of single-beam spectra of glucose samples. In an initial study, partial least-squares (PLS) calibration models were successfully constructed on the basis of the direct use of single-beam spectra.<sup>13</sup> In this previous study, several data sets were studied including aqueous glucose samples in variable protein and variable triacetin matrices. With these data sets, the calibration models based on single-beam spectra were as good as those based on ratioed spectra in absorbance units. This initial success encouraged us to investigate the direct analysis of single-beam spectra further.

Compared to the standard absorbance spectral analysis, the direct analysis of single-beam spectra is complicated by the effects of spectral variation arising from instrumental and environmental changes, as well as the nonlinearity that may exist in the relationship between absolute light intensities and analyte concentrations. These two issues are addressed in this paper. Several data pretreatment methods are evaluated to reduce the effects of day-to-day instrumental variation. Nonlinearities in the relationship between the spectral intensities and analyte concentrations are investigated by use of stepwise quadratic PLS (QPLS) regression. Two different data sets of aqueous glucose samples in matrices of bovine serum albumin (BSA) and triacetin are used in this investigation.

## EXPERIMENTAL

**Design of the Data Sets.** The two data sets employed in this study had the same constituents. In addition to the analyte, glucose, the aqueous samples contained BSA and triacetin. The BSA and triacetin were used to model blood proteins and triglycerides, respectively. Proteins and triglycerides have been identified as major interferences in near-IR blood glucose measurements.<sup>9</sup> The first data set (termed GTB.1) has been employed in previous

Received 9 June 1998; accepted 10 December 1998.

\* Author to whom correspondence should be sent.

studies.<sup>10–12</sup> In a procedure to minimize the correlation among the chemical constituents in the GTB\_1 samples, the concentration levels of glucose, BSA, and triacetin were varied with a factorial design. With this design, a total of 160 samples were prepared consisting of ten levels of glucose (1, 3, 5, 7, 9, 11, 13, 15, 17, and 19 mM), four levels of BSA (50, 65, 80, and 95 g/L), and four levels of triacetin (1.4, 2.1, 2.8, and 3.5 g/L).

A different design method was used for the second data set (termed GTB\_2). For this data set, a genetic algorithm (GA) design program was used to generate the various concentration levels of glucose, BSA, and triacetin.<sup>14</sup> This program constructed samples from a pool of possible concentration levels in such a way as to minimize correlation among the concentrations of the constituents. The data set consisted of 100 samples with glucose levels selected from the range of 1–20 mM at 0.5 mM intervals, BSA levels selected from the range of 49.4–95.0 g/L at 1.9 g/L intervals, and triacetin levels selected from the range of 1.4–3.5 g/L at 0.35 g/L intervals. Fourteen of the samples contained glucose concentrations of 1.0 mM. A large fraction of low-concentration glucose samples and more levels of BSA and triacetin made the glucose analysis of the GTB\_2 data set more challenging than that of the GTB\_1 set.

**Apparatus and Reagents.** The sample preparation, experimental instrumentation, and procedures were similar for both data sets. The samples were prepared by dilution of stock solutions in 0.1 M phosphate buffer at pH 7.4. 5-Fluorouracil (0.044% w/w) was added to the buffer as a preservative for the GTB\_1 data set, while sodium benzoate (0.5% w/w) was used as a preservative for the GTB\_2 case. The glucose (ACS reagent, Fisher Scientific, Fair Lawn, NJ) was dried at 92 °C overnight and then cooled to room temperature in a desiccator. The concentrations of stock solutions for glucose, BSA (Cohn fraction V powder, product no. A4503, Sigma Chemical Co., St. Louis, MO), and triacetin (99%, Sigma Chemical Co.) were 50 mM, 190 g/L, and 35 g/L, respectively, for both data sets.

The spectra for both data sets were collected with a Digilab FTS-60A Fourier transform spectrometer (Bio-Rad, Cambridge, MA). The spectrometer was equipped with a standard near-IR configuration consisting of a 100 W tungsten-halogen source, CaF<sub>2</sub> beamsplitter, and cryogenically cooled indium antimonide (InSb) detector. A K-band optical interference filter (Barr Associates, Westford, MA) was used to isolate the near-IR range of 5000–4000 cm<sup>-1</sup>, which served as the focus of the analysis. The samples were contained in an Infracil quartz cell with a pathlength of 2 mm. Sample temperatures were controlled by use of a water-jacketed cell holder and refrigerated circulator. The temperature was controlled to 37–38 °C during the spectral collection of the GTB\_1 samples, while the temperature for the GTB\_2 samples was controlled to 37 (±0.2) °C. Sample temperatures were measured by use of a type T thermocouple and digital thermocouple meter (Omega Engineering, Stamford, CT).

**Procedures.** The data collection for the GTB\_1 and GTB\_2 data sets spanned 86 and 53 days, respectively. The data sets were collected approximately two years apart. For each GTB\_1 sample, single-sided interferograms containing 16 384 points were collected, and 256

TABLE I. Data set partitioning.

Data set	GTB_1 no. of samples (spectra)	GTB_2 no. of samples (spectra)
Calibration subset	96 (288)	64 (192)
Monitoring set	24 (72)	16 (48)
Calibration set	120 (360)	80 (240)
Prediction set	40 (120)	20 (60)
Total	160 (480)	100 (300)

coadded scans were used. For each GTB\_2 sample, single-sided interferograms containing 8192 points were collected with 512 coadded scans. The spectrometer was aligned and calibrated at the beginning of each day. For both data sets, three replicate spectra were collected consecutively for each sample. The sample order was randomized with respect to concentration to reduce the probability of correlation between glucose concentrations and any time-dependent data artifacts. For both data sets, single-beam spectra were calculated by Fourier processing the collected interferograms with triangular apodization and Mertz phase correction. In addition, one level of zero-filling was applied to the interferograms in the GTB\_2 data set. The resulting single-beam spectra for both data sets had a nominal point spacing of 2 cm<sup>-1</sup>. At the beginning of each data collection session and after approximately each five samples, background spectra of phosphate buffer were collected. The background spectra were used to compute spectra in absorbance units. In this study, the analysis of the computed absorbance spectra was conducted for comparison purposes.

The single-beam spectra for both data sets were transferred to a Silicon Graphics 4D/460 computer (Silicon Graphics, Mountain View, CA) where the spectral data were stored. The data analysis was performed with a Silicon Graphics Indigo<sup>2</sup> R10000 workstation (Silicon Graphics) operating under Irix (Version 6.2). The data analysis software used in this study was implemented in FORTRAN 77. Multiple linear regression and Fourier filtering computations were performed with subroutines from the IMSL software package (IMSL, Houston, TX).

In an effort to build and evaluate optimal multivariate calibration models, both data sets were randomly split into calibration and prediction sets, as shown in Table I. For the GTB\_1 data set, 75% of the samples were put into the calibration set, while the remaining 25% of the total samples were placed into the prediction set. For the GTB\_2 data set, the calibration set consisted of 80% of the whole data set, while the prediction set contained the remaining 20%. For both data sets, the calibration set was randomly divided three times into three calibration subsets (80% of the calibration samples) and corresponding monitoring sets (20% of the calibration samples). The replicate spectra of the samples were placed together into the same set. The optimization of the parameters associated with each calibration model was performed with the use of only the three calibration/monitoring sets. The monitoring sets were employed to evaluate the prediction performance of candidate models computed with the corresponding calibration subsets. The prediction set was an independent data set used to test the performance of the final optimized calibration models.

## RESULTS AND DISCUSSION

**Single-Beam Spectra of the Data Sets.** Unlike spectra in absorbance units, the principal features of single-beam spectra normally consist of background information. The dominant feature of the background is the instrument response function of the spectrometer. In addition, significant absorption of light by the analyte or other components of the sample matrix is observed in the single-beam spectrum in the form of regions of decreased light intensity.

The solid lines in Figs. 1A–1D depict the single-beam spectrum of a phosphate buffer sample. The overall spectral shape in this case is determined by the K-band interference filter used as part of the optical system and the strong absorption bands of water at 5200 and 3800  $\text{cm}^{-1}$ . At the optical pathlength of 2 mm used in the experiment, the water absorbs essentially all light passed by the filter in the region of 5000–4800 and 4200–4000  $\text{cm}^{-1}$ . The dashed lines in Fig. 1 represent the single-beam spectra for glucose in phosphate buffer at 50 mM (A), BSA in buffer at 190 g/L (B), triacetin in buffer at 35 g/L (C), and a GTB\_1 sample (D) consisting of 19 mM glucose, 79.83 g/L BSA, and 2.80 g/L triacetin. For ease of comparison, each single-beam spectrum is plotted by scaling its maximum value to unity. Figure 1A shows that the differences between the single-beam spectra of 50 mM glucose and phosphate buffer solutions are too small to be observed visually. With knowledge that absorption bands of glucose are centered near 4300 (C–H combination), 4400 (C–H combination), and 4700  $\text{cm}^{-1}$  (O–H combination), the absorption by 50 mM glucose is simply too small to alter the appearance of the single-beam spectrum of the water background. Considering that the glucose concentration ranges are from 1 to 20 mM in the GTB data sets, it is clear that the glucose information must be extracted from an overwhelming background if the single-beam spectra are to be analyzed directly. The differences between the single-beam spectra of 190 g/L BSA, 35 g/L triacetin, and phosphate buffer can be observed in Figs. 1B and 1C, respectively. Relative to the buffer spectrum, the visible intensity changes arise from the N–H and C–H combination bands of BSA centered near 4600 and 4370  $\text{cm}^{-1}$ , respectively, and the C–H combination band of triacetin near 4450  $\text{cm}^{-1}$ . The single-beam spectrum of the GTB sample (Fig. 1D) is similar to that of BSA (Fig. 1B). This result illustrates that, in addition to the water background, the protein bands are the dominant spectral features in the GTB data sets.

Another difficulty in the direct analysis of single-beam spectra is the variation in single-beam intensities arising from day-to-day instrumental variations such as the change of alignment of the interferometer and variation in the placement of the sample cell in the spectrometer. Figure 2A shows the single-beam spectra of ten GTB\_1 samples that spanned the approximate intensity range of 21–37 (arbitrary units) for the entire data set. The variation in intensity across the group of single-beam spectra is significant and represents one of the major concerns in the direct analysis of single-beam spectra. In this study, data pretreatment methods are investigated to reduce these single-beam intensity variations.

**Overview of Data Analysis Methods.** For a transmis-

sion measurement, the relationship between light intensity and the concentrations of the absorbing species is described by the Beer–Lambert law. For discrete spectral data, the light intensity can be expressed as

$$x_{i,j} = I_j 10^{-\sum_{k=1}^q \epsilon_{k,j} b c_{i,k}} \quad (1)$$

where  $x_{i,j}$  is the light intensity measured at spectral resolution element  $j$  with sample  $i$  in the optical path; the  $I_j$  term specifies the light intensity measured at resolution element  $j$  in the absence of absorbing species;  $q$  denotes the number of absorbing species;  $\epsilon_{k,j}$  is the absorptivity of species  $k$  at resolution element  $j$ ;  $b$  is the optical pathlength of the measurement; and  $c_{i,k}$  is the concentration of species  $k$  in sample  $i$ .

In the case in which a representative background measurement can be made (i.e., the values of  $I_j$  can be measured), Eq. 1 can be linearized easily to

$$a_{i,j} = -\log\left(\frac{x_{i,j}}{I_j}\right) = \sum_{k=1}^q \epsilon_{k,j} b c_{i,k} \quad (2)$$

where  $a_{i,j}$  is the absorbance of sample  $i$  at resolution element  $j$ . This transformation allows the construction of linear multivariate calibration models that use data at multiple resolution elements to allow the modeling of the components on the right side of Eq. 2 that represent the absorptions of the sample constituents. This approach represents the conventional approach to the design of calibration models for mixture samples containing multiple absorbing species.

The direct analysis of single-beam spectra is motivated in cases in which the values of  $I_j$  are difficult to measure (e.g., a noninvasive glucose measurement). In these cases, a calibration model must be constructed that relates the  $x_{i,j}$  in Eq. 1 to the corresponding  $c_{i,k}$ .

If a constant of  $I_j = 1$  is assumed for all  $j$  across all samples, the log transform of Eq. 2 can be performed and a conventional linear multivariate calibration model can be computed.<sup>15,16</sup> Figure 2B plots the single-beam spectra of Fig. 2A after the log transform. It is clear that in addition to the potential linearization of the relationship between the  $x_{i,j}$  and  $c_{i,k}$ , the transform reduces the magnitude of the intensity variation across the spectra.

If the values of  $\epsilon_{k,j} b c_{i,k}$  are small, the  $x_{i,j}$  can be used directly to build a conventional calibration model. This approach exploits the Maclaurin series expansion of  $10^{-x} \approx 1 - x$  for small  $x$ . In practice, however, neither of these strategies is entirely appropriate, and the resulting calibration models must attempt to overcome the intrinsic nonlinearity of Eq. 1 and the inability to correct for variation in  $I_j$  from day to day and sample to sample.

To help overcome these problems, one can use a combination of approaches. First, preprocessing methods can be employed to remove artifacts from the measured intensity values. In the work reported here, three of these methods are evaluated: multiplicative signal correction (MSC), spectral normalization, and digital filtering.

The MSC method is also called multiplicative scatter correction and was originally developed to correct the effects of light scattering in reflectance spectroscopy.<sup>17–20</sup> Just as light scattering effects can induce overall changes in light intensity in reflectance spectra, day-to-day variations in interferometer alignment and sample cell positioning can cause similar variations in the absolute single-

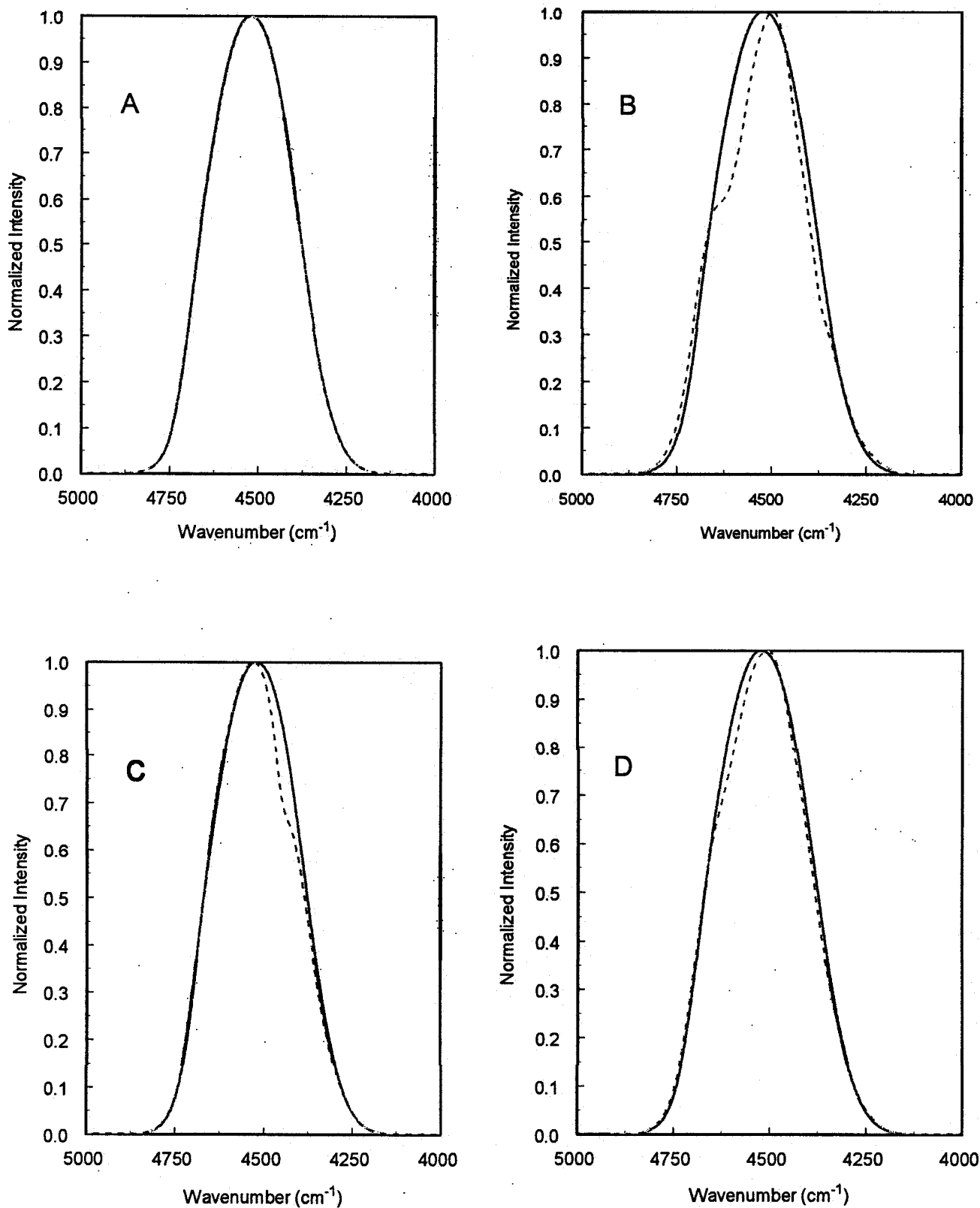


FIG. 1. Normalized near-IR single-beam spectra. Solid lines in A–D represent spectra of phosphate buffer. Dashed lines are for 50 mM glucose (A); 190 g/L BSA (B); 35 g/L triacetin (C); and a GTB-1 sample (19 mM glucose, 79.83 g/L BSA, and 2.80 g/L triacetin) (D), respectively.

beam spectral intensities measured in a transmission experiment. In this research, MSC was used to help correct this intensity variation in the single-beam spectra. For the implementation of MSC, the mean spectrum of the cali-

bration set (or calibration subset) is commonly used as a reference spectrum. The spectrum of each sample is then regressed against the mean spectrum to produce the model shown in Eq. 3:

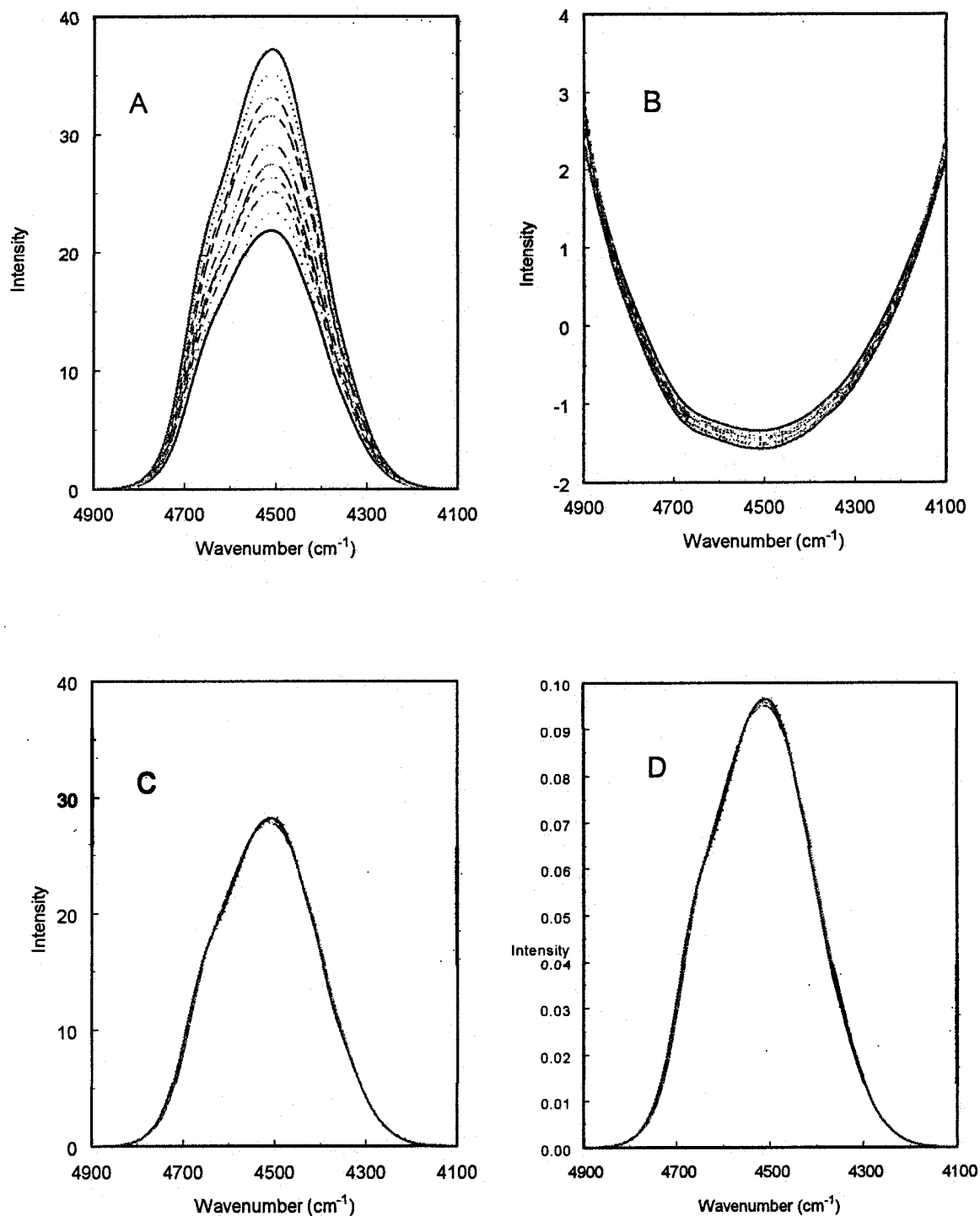


FIG. 2. (A) Single-beam spectra of ten samples in the GTB.1 data set; (B) log-transformed single-beam spectra from those in (A); (C) MSC-corrected single-beam spectra from those in (A); and (D) normalized single-beam spectra from those in (A).

$$x_{i,j} = a_i + b_i \bar{x}_j + e_{i,j}. \quad (3)$$

The value of  $\bar{x}_j$  is the mean intensity value of the calibration set (or calibration subset) at resolution element  $j$ , and  $e_{i,j}$  is the residual of the model for sample  $i$  at resolution element  $j$ . Computed across a set of resolution elements, the intercept ( $a_i$ ) and the slope ( $b_i$ ) encode additive and multiplicative effects, respectively, that relate the spectrum of sample  $i$  to the mean spectrum. It is assumed that these effects are general trends and are not

related to the chemical information. Removal of these trends is thus accomplished by

$$x_{i,j} \text{ corrected} = (x_{i,j} - a_i)/b_i. \quad (4)$$

The mean spectrum of the calibration set is also used to correct spectra in the prediction set to which the calibration model will be applied.

Figure 2C shows the MSC-corrected single-beam spectra of the ten GTB.1 samples that are displayed in Fig.

2A. Compared to Fig. 2A, the single-beam intensity variation is greatly reduced in the MSC-corrected spectra.

A normalization method was also used to remove the single-beam intensity variation. In this study, the single-beam spectra were normalized by dividing the values of individual spectral points by the root sum of squares of the intensity values in the corresponding spectrum. This calculation can be expressed as

$$x_{i,j,\text{normalized}} = \frac{x_{i,j}}{\sqrt{\sum_{j=1}^p x_{i,j}^2}} \quad (5)$$

where  $p$  is the number of resolution elements in a specified range of the spectrum for sample  $i$ . The normalized single-beam spectra of the original ten spectra in Fig. 2A are shown in Fig. 2D. Similar to the case for MSC-corrected spectra, the intensity variation is largely removed in the normalized single-beam spectra.

An assumption inherent in both the normalization procedure described above and in the MSC method is that the overall light intensity in the spectral region used to define the normalizing constants is independent of the absorbance of the varying constituents of the sample matrix. This assumption is valid in the present application because of the small absorbance of glucose, triacetin, and BSA relative to the large water absorbance. Stated differently, the overall spectral intensity should be almost constant from sample to sample because of the almost constant water absorbance. For this reason, a broad range of 4900–4100  $\text{cm}^{-1}$  was used in this work to implement both MSC and normalization calculations. In other applications in which large intensity variations are induced by the absorbance of the matrix constituents, the spectral range over which the normalizing constants are computed must be chosen with care.

Bandpass Fourier digital filtering was also employed to remove unwanted variation in the single-beam spectra. Spectra were windowed with a cosine windowing function before the filtering step in order to help prevent artifacts from being introduced into the filtered spectra through the Fourier transform operations. In applying bandpass filtering, the single-beam spectrum is represented by its underlying harmonic frequencies. Chemical information can be isolated on the basis of its difference in frequency content as compared to other sources of spectral variation. The frequency is linearly scaled to a range 0–0.5  $f$  (digital frequency units). Noise information is located largely in the high-frequency region, and any baseline variations are concentrated at low digital frequencies. Information about the absorptions of the sample constituents dominates the middle range of frequencies. With the use of a Gaussian-shaped bandpass function, the chemical information may be enhanced by suppressing the other sources of variation.

In conjunction with appropriate preprocessing methods, the construction of the calibration model can be performed to suppress information in the intensity data that is not relevant to modeling the analyte concentrations. Principal component analysis (PCA) and partial least-squares are methods that can be used with the original  $x_{i,j}$  to construct latent variables that are biased to suppress variation in the data that is likely not to be useful in

modeling the analyte concentrations.<sup>17</sup> The PLS method was used in this work and was applied to the mean-centered spectral data in both a conventional linear multivariate calibration model and as a quadratic model (QPLS).

The QPLS regression method is designed to help model the nonlinear relationship between the dependent and independent variables that is suggested by Eq. 1. In the case with only one dependent variable (glucose concentration), the first step of QPLS is the same as linear PLS. In this step, the single-beam spectral intensity data matrix [ $n$  (spectra)  $\times$   $k$  (resolution elements)] is decomposed into a matrix of lower dimensionality ( $n \times h$ ) by considering the covariance between the spectral intensities and the analyte concentrations. The resulting PLS scores are orthogonal so that the colinearity among the independent variables that exists in the original data matrix is removed in the score matrix.

The second step of QPLS regression is different from that of linear PLS regression. The QPLS regression model has the form

$$c_i = b_0 + b_1 t_{i,1} + \dots + b_h t_{i,h} + b_{h+1} t_{i,1}^2 + \dots + b_{2h} t_{i,h}^2 \quad (6)$$

where  $c_i$  is the predicted concentration for sample  $i$ , the  $t_i$  values are the computed PLS scores, the  $b$  terms are regression coefficients, and  $h$  is the number of latent variables (PLS factors). In Eq. 6, note that quadratic polynomial terms based on the PLS scores are included in the QPLS regression.

Stepwise QPLS is a parsimonious version of QPLS regression in which only the statistically significant terms in Eq. 6 are included in the calibration models. This method has been used successfully in previous work with spectra in absorbance units.<sup>22</sup> The stepwise QPLS method implemented here consisted of a combination of forward stepwise addition and backward deletion. Terms were added to the model one at a time if they met a significance level of 0.05 ( $F$ -test). Once a new term was added, the significance levels of previously added terms were updated. Previously added terms were deleted if their significance levels fell below 0.05. The specific  $F$ -test used was based on the values of the partial  $F$ -test statistic. This statistic evaluates whether the reduction in the error sum of squares afforded by adding the term to the model is significant.<sup>23</sup>

**Analysis of Single-Beam Spectra without Digital Filtering.** As discussed before, in order to implement successful multivariate calibration models for the direct analysis of single-beam spectra, two issues need to be addressed. One is the effect of the single-beam intensity variation caused by uncontrollable instrumental changes. The other is the nonlinear relationship between the single-beam intensities and the analyte concentrations. To investigate the effects of these two factors on the analysis of the single-beam spectra, we employed both linear PLS and stepwise QPLS methods to build the calibration models for the GTB\_1 and GTB\_2 data sets. To compare with the models based on the use of the original single-beam spectra, we also used the data pretreatment methods discussed previously (i.e., log transform, MSC, and nor-

malization) for preprocessing the single-beam spectra to reduce the variation in spectral intensity.

Analogous to the optimization procedure used for selecting PLS models based on absorbance spectra, the spectral range and the number of PLS factors need to be optimized for calibration models computed with single-beam spectra. A grid search procedure was adopted to optimize these PLS model parameters. To study the effect of various spectral ranges, we varied the size and location of the range in a systematic manner. The size of the spectral range was changed from 700 to 200  $\text{cm}^{-1}$  by decrements of 50  $\text{cm}^{-1}$ . For a given range size, the spectral range was shifted across the region of 4900–4100  $\text{cm}^{-1}$  in steps of 25  $\text{cm}^{-1}$ . With each selected spectral range, the number of PLS factors was varied from 5 to 20. Candidate models based on each selected spectral range and number of PLS factors were built with the use of three different calibration subsets, and their prediction performance was evaluated with the use of three corresponding monitoring sets. The pooled standard error of monitoring (SEM) was used to determine the optimal calibration models. For one monitoring set, the SEM can be calculated by

$$\text{SEM} = \sqrt{\frac{\sum_{i=1}^{n_m} (c_{i,m} - \hat{c}_{i,m})^2}{n_m}} \quad (7)$$

where  $c_{i,m}$  and  $\hat{c}_{i,m}$  are the actual and predicted analyte concentrations for spectrum  $i$ , respectively, and  $n_m$  is the number of spectra in the monitoring set.

A significance testing procedure analogous to that proposed by Haaland and Thomas<sup>24</sup> was used to select the optimal number of PLS factors. For each selected spectral range, the number of PLS factors that produced the minimum pooled SEM across the three monitoring sets was found first. Then the SEM of a model based on one fewer PLS factor was compared to the minimum SEM by use of an  $F$ -test at a 95% confidence level. Unless a significant difference was found between the selected SEM and the minimum SEM, the procedure continued with progressively smaller models. The smallest model that produced an SEM not significantly different from the minimum SEM was used.

Once the optimal models were selected, the full calibration set was used to build the final model. The performance of the optimal models was tested with the independent prediction set. The procedure described above for selecting the optimal models was used for both linear PLS and stepwise QPLS regression with the various data preprocessing methods.

The top five spectral ranges and corresponding optimal number of PLS factors were selected to build the final models with the calibration set. These models were subsequently applied to predict the glucose concentrations corresponding to the spectra in the prediction set. For the GTB.1 data set, among the five optimal models, the one which provided the lowest standard error of prediction (SEP) is reported in Table II. Along with the SEP values, Table II lists the spectral range, the number of PLS factors (plus the number of quadratic terms for the QPLS models), and the standard error of calibration (SEC). The calculation of SEC and SEP is analogous to Eq. 7, with

TABLE II. Results without filtering for the GTB.1 data set.

Method <sup>a</sup>	Spectral range ( $\text{cm}^{-1}$ )	No. of PLS factors (+quadratic terms)	SEC <sup>b</sup> (mM)	SEP <sup>c</sup> (mM)
PLS (absorbance)	4725–4275	17	0.41	0.61
PLS (sb)	4700–4200	15	0.74	0.72
PLS/log	4750–4275	15	0.52	0.62
PLS/MSC	4750–4200	15	0.53	0.59
PLS/norm	4700–4300	14	0.57	0.60
QPLS	4700–4200	15 (+3)	0.72	0.72
QPLS/log	4725–4300	17 (+4)	0.40	0.55
QPLS/MSC	4800–4200	15 (+7)	0.47	0.52
QPLS/norm	4800–4150	12 (+2)	0.48	0.54

<sup>a</sup> sb or no indication denotes that the method is based on the use of single-beam spectra. PLS/log, PLS/MSC, and PLS/norm are the combinations of PLS regression and log transform, MSC, and normalization, respectively. The same representations are used for the stepwise QPLS models.

<sup>b</sup> Standard error of calibration.

<sup>c</sup> Standard error of prediction.

the exception that, for the case of SEC, the degrees of freedom are reduced by the number of terms in the model.

The grid search optimization procedure described above was also used with absorbance spectra, and the results from the model that produced the lowest SEP are listed in the first row of Table II. Background spectra of phosphate buffer were used in converting the single-beam spectral intensities to absorbance units. In computing the absorbance values for each sample spectrum, the most recently collected background spectrum was used.

The other results in Table II correspond to the optimal models obtained from the analysis of single-beam spectra. In the method column, PLS (sb) denotes that a linear PLS model was built with the use of the original (i.e., unprocessed) single-beam spectra in the GTB.1 data set. PLS/log denotes that the PLS model was constructed with the log-transformed single-beam spectra. Similarly, PLS/ MSC and PLS/norm indicate that the PLS models were based on the MSC-corrected and normalized single-beam spectra, respectively. The same notation is used for the representation of the preprocessing methods employed with the stepwise QPLS models.

Compared to the results obtained with the optimal PLS model based on absorbance spectra, the performance of the model computed with the unprocessed single-beam spectra was not good. The degraded performance of this model was caused by the significant variation in the single-beam spectral intensities. By a reduction in this intensity variation with the data pretreatment methods, the prediction results of the optimal PLS models were all significantly improved compared to the model based on no preprocessing. Encouragingly, the best results obtained with the preprocessed single-beam spectra are slightly better than those obtained with the model computed with absorbance spectra. This result suggests that, with the sample matrix used here, the single-beam spectrum of phosphate buffer may not be sufficiently representative of the true background to provide an advantage when it is used to define the  $I_j$  values in Eq. 2.

The results obtained with the optimal QPLS models built with the use of the unprocessed single-beam spectra were about the same as those obtained with the linear

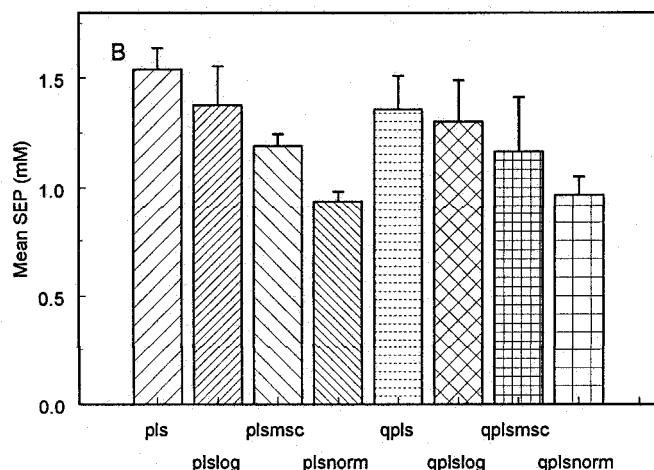
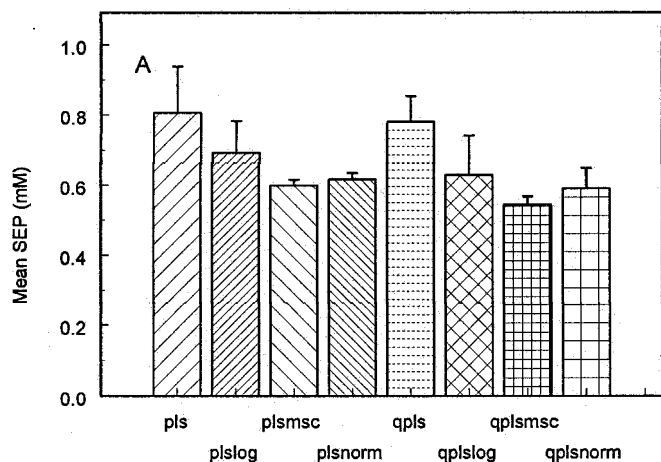


FIG. 3. Mean SEP values and the corresponding upper 95% confidence limits (error bars) from the top five models obtained through the use of unfiltered single-beam spectra with various data analysis methods. (A) GTB.1 data set; (B) GTB.2 data set.

PLS models. However, with the use of preprocessed single-beam spectra, the optimal stepwise QPLS models yielded lower SEP values than the corresponding linear PLS models.

The SEP values listed in Table II were also compared to each other by converting them to the corresponding variance estimates and then computing  $F$ -values and associated probabilities from the  $F$  cumulative distribution function. From these comparisons, the following conclusions were drawn: (1) the QPLS methods with preprocessing yielded prediction results that were better than the results from the analysis of absorbance spectra at significance levels greater than 87%, but the results obtained with the different preprocessing methods were not significantly different from each other; (2) for each of the preprocessing methods, the QPLS results were better than the corresponding linear PLS results at significance levels of at least 87%; and (3) all the PLS and QPLS methods with preprocessing were better than the PLS and QPLS methods with no preprocessing at significance levels greater than 94%.

Figure 3A displays the mean SEP values obtained from the top five calibration models along with error bars drawn at the upper 95% confidence limits for the various

TABLE III. Results without filtering for the GTB.2 data set.

Method <sup>a</sup>	Spectral range (cm <sup>-1</sup> )	No. of PLS factors (+quadratic terms)	SEC <sup>b</sup> (mM)	SEP <sup>c</sup> (mM)
PLS (absorbance)	4700–4325	13	1.16	1.09
PLS (sb)	4700–4200	16	1.02	1.49
PLS/log	4800–4300	17	0.95	1.16
PLS/MSC	4900–4200	15	0.91	1.12
PLS/norm	4875–4175	16	0.79	0.89
QPLS	4850–4250	16 (+5)	0.98	1.18
QPLS/log	4625–4250	14 (+2)	0.97	1.06
QPLS/MSC	4900–4200	15 (+5)	0.85	0.89
QPLS/norm	4875–4275	16 (+3)	0.82	0.86

<sup>a</sup> The same representations are used as in Table II.

<sup>b</sup> Standard error of calibration.

<sup>c</sup> Standard error of prediction.

data processing methods applied to the single-beam spectra from the GTB.1 data set. Again, the prediction results from the models (PLS and QPLS) with all the pretreatment methods (i.e., log transform, MSC, and normalization) were significantly better than those obtained without the use of preprocessing. The mean SEP values obtained with the QPLS models with the log transform and normalization were not significantly improved compared to the corresponding linear PLS models. However, the QPLS models with MSC-corrected single-beam spectra performed better than the corresponding linear PLS models.

The same optimization procedure and data analysis methods were applied to the GTB.2 data set. The optimal results from the various methods are reported in Table III. The mean SEP values provided by the top five calibration models computed from the single-beam spectra of the GTB.2 data set are shown in Fig. 3B. As in Fig. 3A, the error bars denote the corresponding upper 95% confidence limits.

The overall results for the GTB.2 data set were not as good as those obtained with the GTB.1 data set. This outcome is reasonable because the GTB.2 data set was designed with more concentration levels of the sample components and had many samples with a low glucose concentration of 1 mM. Similar to the results for the GTB.1 data set, the performance of the optimal linear PLS model built with unprocessed single-beam spectra was significantly worse than that obtained with the absorbance spectra. The use of the data pretreatment methods improved the model performance with the single-beam spectra. For the optimal results listed in Table III, the improvement of the QPLS models over the corresponding linear PLS models was observed. However, the mean SEP values displayed in Fig. 3B did not show this improvement.

Statistical comparisons of the SEP results in Table III were also performed by use of computed  $F$ -values and associated probabilities. Results similar to those described previously were obtained. At significance levels greater than 94%, the QPLS methods with MSC and normalization yielded better results than the corresponding analysis of absorbance spectra, but the results with MSC and normalization were not significantly different from each other. Unlike the case of the GTB.1 data set, however, the QPLS method with log preprocessing did not

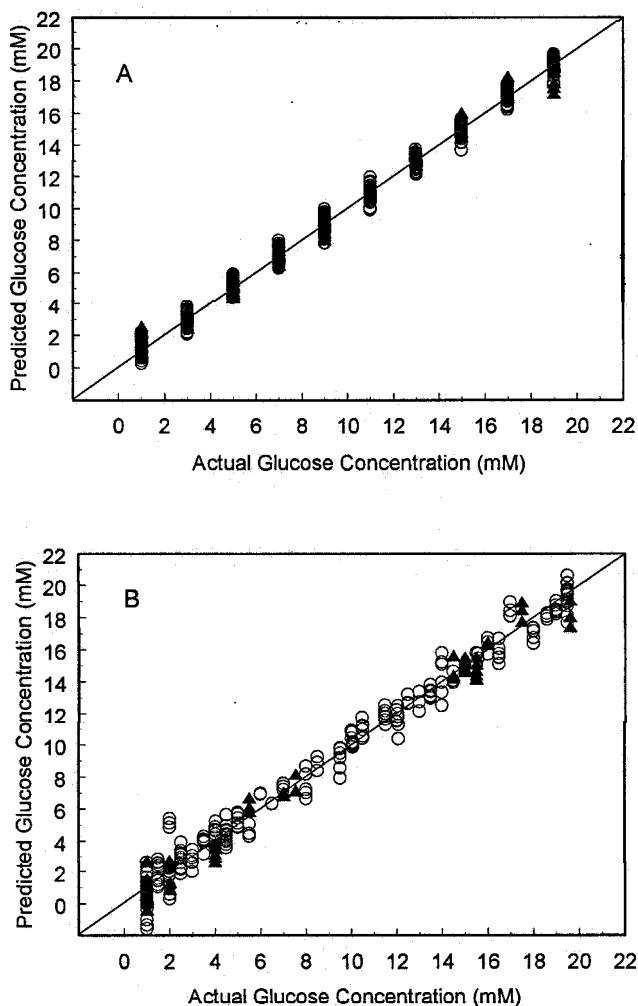


FIG. 4. Concentration correlation plots with the optimal stepwise QPLS models with the MSC-corrected single-beam spectra. (A) GTB.1 data set; (B) GTB.2 data set.

perform significantly better than the analysis of absorbance spectra. All PLS and QPLS methods with preprocessing performed better than PLS without preprocessing at significance levels greater than 96%, while the QPLS methods with MSC and normalization performed better than QPLS with no preprocessing at significance levels greater than 98%.

Figures 4A and 4B show concentration correlation plots for the GTB.1 and GTB.2 data sets, respectively. The plots were based on the optimal QPLS models computed with MSC-corrected single-beam spectra. Both plots indicate that good correlation was found between the predicted and actual glucose concentrations.

**Analysis of Digitally Filtered Single-Beam Spectra.** The combination of digital Fourier filtering with the data pretreatment methods discussed in the previous section was employed for building both linear PLS and stepwise QPLS models with the GTB.1 and GTB.2 data sets. In this work, the pretreatment methods were applied first, followed by the filtering step.

The use of digital filtering as the preprocessing method added two more parameters to be optimized, the position and width of the Gaussian-shaped bandpass function. The grid search procedure employed in the previous section

for selecting the spectral range and the number of PLS factors becomes very time-consuming if the filter position and width parameters are added. Because of this limitation, a more efficient optimization protocol based on a genetic algorithm has been developed in our laboratories for the joint optimization of the parameters involved in combining digital filtering with PLS regression.<sup>10</sup> This GA-based procedure was adopted in this study to optimize the model parameters associated with the use of digitally filtered single-beam spectra.

GAs are numerical optimization methods based on the concepts of genetics and natural selection.<sup>25-27</sup> The individual variables to be optimized are termed genes, and the set of variables is called a chromosome. In this application, the chromosome consisted of five genes (filter position, filter width, number of PLS factors, starting point, and ending point of the spectral range), each represented as an integer. The continuous filter position and width parameters were converted to an integer representation by mapping the range of 0.0 to 0.2  $f$  onto a series of integers through the use of a fixed resolution of 0.0001  $f$ . This range was restricted to 0.1  $f$  in our previously published work because we have rarely found filter positions and widths greater than 0.1  $f$  to be useful when applied to absorbance spectra at the nominal 2  $\text{cm}^{-1}$  point spacing used here. However, with the use of single-beam spectra, some filters with positions and/or widths larger than 0.1  $f$  were found to be useful. Therefore, the range for the filter position and width was extended to 0.2  $f$  in this study.

The fitness function chosen to guide the GA optimization was originally developed for the analysis of absorbance spectra.<sup>10</sup> This function is defined as

$$(\text{MSE} + \text{MSME} + h^w)^{-1} \quad (8)$$

where MSE represents the mean-squared error in concentration of the spectra in the calibration subset, MSME is the mean-squared error in concentration obtained when the computed calibration model is applied to the spectra in the monitoring set,  $h$  is the number of PLS factors employed in the calibration model, and  $w$  is a weighting factor. In practice, three different calibration subsets and monitoring sets were randomly selected during the optimization procedure. The mean value of Eq. 8 obtained with these three rearrangements of the data set was used as the fitness value of each chromosome. By use of this fitness function, the models judged optimal by the GA achieved a balanced calibration and prediction performance and required as few PLS factors as possible. In the original work in which Eq. 8 was developed, weighting factors of 0.2 and 0.6 were found to be optimal for the GTB.1 and GTB.2 data sets, respectively, as these values produced models that achieved a balance between a low SEM and a small number of PLS factors.<sup>10</sup>

The GA configuration parameters employed for the GTB.1 and GTB.2 data sets are listed in Table IV. The configuration parameters were chosen on the basis of the previous study that employed absorbance spectra<sup>10</sup> and were not optimized further. A larger number of generations was used with the GTB.2 data set because it contained fewer spectra than the GTB.1 set. Three GA runs were performed by using different starting chromosomes for each data set. The parameters in the five chromo-

TABLE IV. Optimal genetic algorithm parameters.

Parameters	GTB_1	GTB_2
Population size	50	50
No. of generations	50	100
Recombination probability	0.9	0.9
Mutation probability	0.1	0.1
Crossover scheme	single-point	single-point

some producing the highest fitness values among the three GA runs were selected to build the final models with the full calibration set as described in the previous section. The prediction set was used to validate the performance of these final models.

For the GTB\_1 data set, the optimal results obtained from the combination of filtering, the pretreatment methods, and the linear and quadratic PLS modeling techniques are listed in Table V. The mean SEP values from the five optimal models and their corresponding upper 95% confidence limits are displayed in Fig. 5A. The optimal model performance obtained with the various preprocessing methods combined with filtering is similar to that obtained with the corresponding methods without filtering. However, the number of PLS factors required for the optimal models was reduced for most of the models constructed with the filtered data. The filtering step simplifies the model because it removes variation that no longer has to be explained by the PLS scores.

Statistical comparisons of the SEP values in Table V were also performed by use of the procedures described previously. All PLS and QPLS methods with log, MSC, or normalization outperformed PLS without these preprocessing steps at significance levels of greater than 95%. Also, the methods of preprocessing were not significantly different from each other for use with either the PLS or QPLS models. These results suggest that while the digital filtering step is useful in removing certain types of spectral variation and can lead to models with fewer terms, it does not take the place of the conventional normalization methods for reducing overall variation in the single-beam spectral intensities.

Table VI lists the optimal results for the GTB\_2 data set. Figure 5B shows the corresponding mean SEP values and the associated upper 95% confidence limits. Again, the overall results obtained with the optimal models with filtering are similar to those produced by the corresponding methods without filtering. As with the GTB\_1 set, smaller model sizes were required for the case in which filtered data were used. Interestingly, the confidence intervals of the SEP values were reduced for models built with filtered data. This observation indicates that the group of calibration models computed with filtered data performs more consistently than the corresponding group of models constructed with unfiltered data. Furthermore, with filtering, the prediction results from the linear PLS models with the log transform and stepwise QPLS models with MSC were improved. This result made the overall pattern of model performance of the various methods obtained with the GTB\_2 data set consistent with that of the GTB\_1 data set.

Statistical comparisons of the SEP values in Table VI revealed that for five of the six cases (i.e., log, MSC, and normalization combined with PLS and QPLS), the PLS

TABLE V. Results with filtered spectra for the GTB\_1 data set.

Method <sup>a</sup>	Spectral range (cm <sup>-1</sup> )	Filter position and width ( <i>f</i> )	No. of PLS factors (+quadratic terms)	SEC <sup>b</sup> (mM)	SEP <sup>c</sup> (mM)
PLS	4715–4100	0.0832 0.0559	17	0.71	0.71
PLS/log	4705–4290	0.0676 0.0297	14	0.49	0.57
PLS/MSC	4740–4200	0.0690 0.0216	13	0.48	0.58
PLS/norm	4720–4235	0.0923 0.0324	12	0.50	0.59
QPLS	4690–4300	0.0366 0.0074	13 (+7)	0.65	0.61
QPLS/log	4705–4300	0.0612 0.0256	13 (+7)	0.46	0.56
QPLS/MSC	4900–4110	0.0660 0.0231	13 (+2)	0.46	0.54
QPLS/norm	4900–4110	0.0765 0.0250	12 (+3)	0.46	0.59

<sup>a</sup> The same representations are used as in Table II.

<sup>b</sup> Standard error of calibration.

<sup>c</sup> Standard error of prediction.

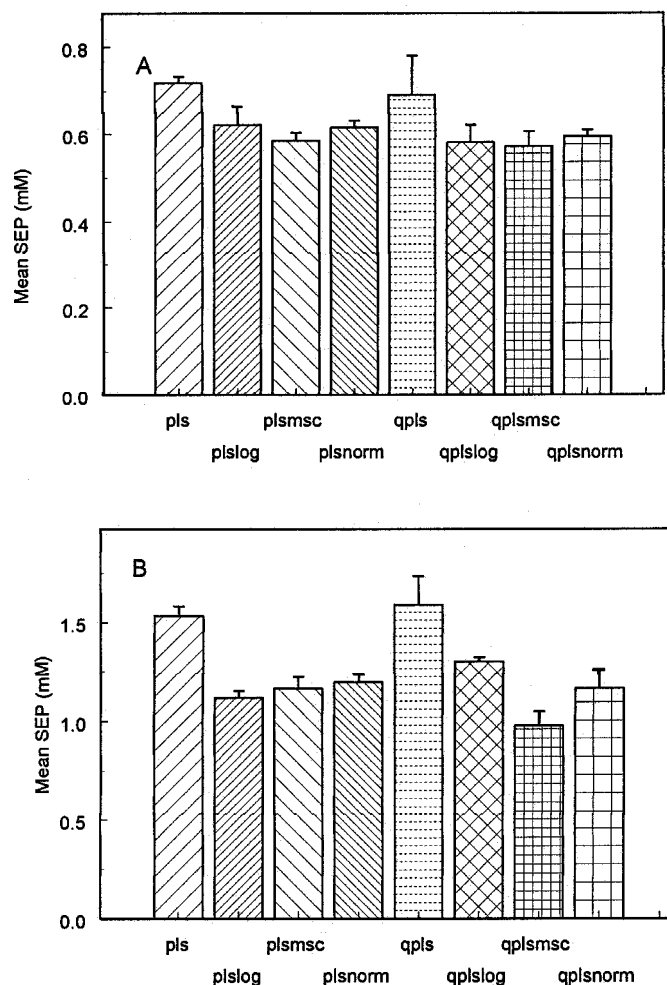


FIG. 5. Mean SEP values and the corresponding upper 95% confidence limits (error bars) from the top five models obtained with filtered single-beam spectra and with various methods of data processing. (A) GTB\_1 data set; (B) GTB\_2 data set.

TABLE VI. Results with filtered spectra for the GTB.2 data set.

Method <sup>a</sup>	Spectral range (cm <sup>-1</sup> )	Filter position and width ( <i>f</i> )	No. of PLS factors (+quadratic terms)	SEC <sup>b</sup> (mM)	SEP <sup>c</sup> (mM)
PLS	4700–4100	0.1792 0.0912	14	1.05	1.48
PLS/log	4625–4345	0.0905 0.0956	10	1.20	1.08
PLS/MSC	4650–4100	0.1246 0.0433	12	0.99	1.09
PLS/norm	4610–4120	0.1124 0.0407	11	1.08	1.17
QPLS	4730–4180	0.1355 0.0581	15 (+6)	0.86	1.49
QPLS/log	4715–4295	0.0974 0.0561	12 (+5)	0.89	1.28
QPLS/MSC	4665–4205	0.0897 0.0347	12 (+5)	0.88	0.92
QPLS/norm	4610–4255	0.1200 0.0465	12 (+3)	0.95	1.05

<sup>a</sup> The same representations are used as in Table II.

<sup>b</sup> Standard error of calibration.

<sup>c</sup> Standard error of prediction.

and QPLS methods with preprocessing outperformed PLS with no preprocessing at significance levels greater than 96%. For the sixth case, the significance level was greater than 86%. For the PLS models, there was no significant difference among the preprocessing methods, while for the QPLS models, MSC and normalization outperformed the log preprocessing method at significance levels of greater than 99%.

**Evaluation of Robustness of Calibration Models.**

All the results presented above were based on the case in which the set of calibration spectra spanned the prediction spectra in time. This approach ensured that the calculation of the calibration models included information about the entirety of the variation in the spectral backgrounds. A more difficult case is one in which the spectra in the prediction set lie outside the time span of the calibration data. In this situation, the calibration model must be robust enough to operate outside its effective knowledge base of spectral backgrounds. This is also the case in which an analysis of absorbance spectra would be expected to have the greatest potential advantage over an analysis of single-beam spectra, since the act of ratioing to a collected background spectrum is at least an attempt to remove the background contribution before the calibration model is applied.

To evaluate this calibration/prediction scenario fully is beyond the scope of the current research since it would require a spectral data set collected in a systematic manner with respect to time. The importance of this issue warrants at least a limited evaluation with the present data, however.

Of the two data sets employed in this research, the GTB.1 set spanned the greatest time and was therefore used in this study. A new partitioning of the data was used in place of that described in Table I. A total of 159 of the original 160 samples were used, corresponding to a time span of 65 days. The one sample removed was collected 21 days after the remainder of the data. Since only a single sample was collected on this day, it was

judged that any results obtained from the use of this sample would be inconclusive.

The first 139 samples collected were placed into the calibration set, while the last 20 samples formed the prediction set. The calibration set was further subdivided into a calibration subset consisting of the first 118 of the 139 samples collected and a monitoring set containing the last 21 (of the 139) samples measured. The 118 samples were collected in 15 data collection sessions spanning 59 days, while the 21 samples in the monitoring set were collected during three data collection sessions that spanned six days. The 20 samples that comprised the prediction set were collected during two data collection sessions that spanned two days. The last data collection session of the calibration subset coincided with the first data collection session of the monitoring set. The first of the 10 samples collected during this session was placed in the calibration set, and the remaining 9 samples were placed in the monitoring set. Similarly, the last data collection session corresponding to the full calibration set (i.e., the last session included in the monitoring set) coincided with the first data collection session used to define the prediction set. The first of the 11 samples collected during this session was included in the full calibration set, and the remaining 10 samples were placed in the prediction set. As before, the replicate spectra corresponding to each sample were carried together into the appropriate data set.

The same preprocessing and model building strategies described previously were used for this study with the exception that no digital filtering was performed. The same grid search optimization procedures were also used except that a different strategy was employed for sorting the results. Since only a single calibration/monitoring set was available, an overall response function, *R*, was computed as

$$R = (SEC + SEM)/2 + |SEC - SEM| \quad (9)$$

where a minimum value of *R* is optimal, and the SEC and SEM values describe the results obtained with the calibration subset and monitoring set, respectively. The inclusion of the |SEC - SEM| term was designed to reduce the ranking of models that had a large discrepancy between the SEC and SEM values.

For each spectral preprocessing and modeling combination, the results obtained from the grid search optimization were sorted by use of Eq. 9, the top five model parameters were selected, and final calibration models were computed by use of the full calibration set. The five resulting models were applied to the prediction set. For the various preprocessing and modeling combinations, Table VII summarizes the minimum, maximum, and mean SEP values obtained from these five sets of prediction results.

Also listed in Table VII are two sets of results for absorbance spectra. The first row in the table lists results obtained with absorbance spectra in which the most recently collected background spectrum was used to compute the absorbance values. This is the routine procedure that was used in the generation of the spectra in the calibration set and in computing all results with absorbance spectra presented previously in Tables II and III.

The second line in Table VII lists results obtained with

**TABLE VII. Prediction results from study of robustness of calibration models.**

Method <sup>a</sup>	Minimum SEP <sup>b</sup> (mM)	Maximum SEP (mM)	Mean SEP (mM)
PLS (absorbance)	0.63	0.95	0.80
PLS (absorbance, single background)	0.68	1.05	0.85
PLS (sb)	1.55	2.59	1.98
PLS/log	0.65	0.94	0.73
PLS/MSC	0.89	1.09	0.97
PLS/norm	0.81	1.32	1.09
QPLS	1.50	2.48	1.83
QPLS/log	0.95	2.36	1.59
QPLS/MSC	0.79	1.13	0.98
QPLS/norm	0.67	1.06	0.94

<sup>a</sup> The same representations are used as in Table II.

<sup>b</sup> Standard error of prediction.

the same calibration model, but for the case in which all absorbance values for the spectra in the prediction set were computed with a single background spectrum. The spectrum used was the first spectrum of phosphate buffer collected during the first of the two data collection sessions used to define the prediction set.

The minimum SEP values in Table VII can be compared to the corresponding SEP results in Table II. The results in Table II represent the ideal case in which the calibration set spanned the prediction set in time. An inspection of Table VII reveals some degradation of results relative to those in Table II. Use of a suboptimal background spectrum in computing absorbance spectra is also observed to degrade the prediction results. However, the best results obtained with single-beam spectra are still on par with those obtained with absorbance data. Compared to the results in Table II, the spectral preprocessing methods are observed to be even more essential for use with the single-beam data.

For the spectra in the prediction set, Fig. 6 plots concentration residuals vs. the time since the collection of the last calibration spectrum for four cases corresponding to the lowest SEP values in Table VII. Included are results from the PLS/log (A) and QPLS/norm (B) models based on single-beam spectra, along with the model based on absorbance spectra in which the spectra in the prediction set were computed with multiple background spectra (C) and a single background spectrum (D). The traces of the residuals show no obvious relationship with time, and the models based on single-beam and absorbance spectra are observed to perform similarly.

## CONCLUSION

Statistical comparisons of the prediction results obtained in this study support the conclusion that, with appropriate preprocessing to remove spectral intensity variation that is unrelated to changes in the concentrations of the sample constituents, the direct analysis of single-beam spectra can yield calibration results that are highly competitive with those produced by a conventional analysis of absorbance spectra. For the specific example used in this research, the results from the analysis of single-beam spectra were in fact statistically better than the corresponding results produced in the analysis of absorbance spectra when the calibration set spanned the prediction

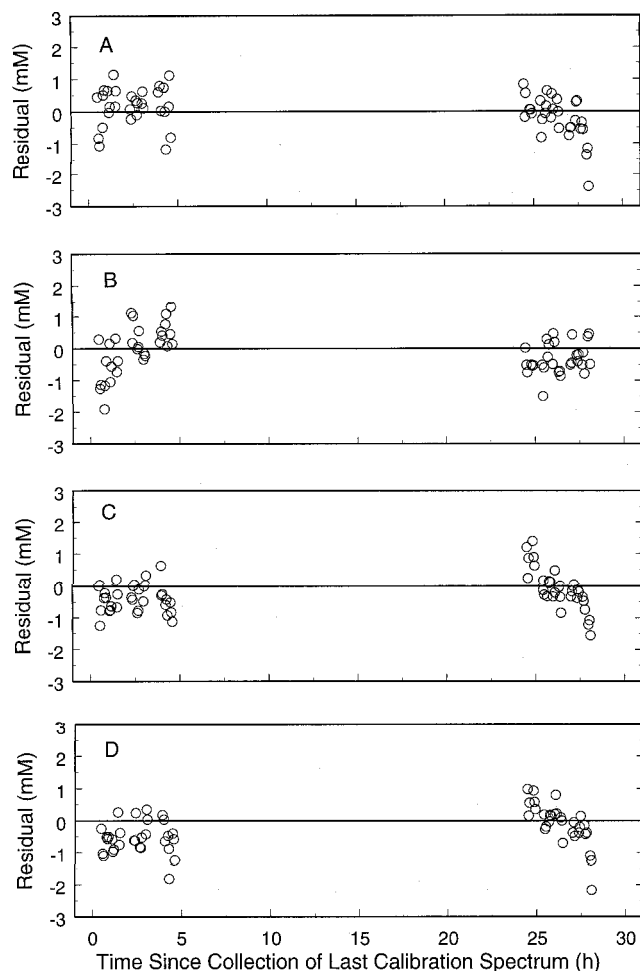


**FIG. 6.** Concentration residuals (mM) for the spectra in the prediction set are plotted vs. the time (h) since the collection of the last calibration spectrum for four cases that yielded the best SEP values. Results are displayed for the PLS/log (A) and QPLS/norm (B) models based on single-beam spectra. Results with absorbance spectra are plotted for the case in which multiple background spectra were used to compute the absorbance values (C) and the case in which a single background spectrum was used (D).

set in time. With the removal of the problematic intensity variation through one of the normalization methods, the analysis of single-beam spectra is found to be a viable alternative approach to the conventional absorbance spectral analysis with the advantage of no requirement for the collection of matching background spectra. This can be an important advantage in measurement scenarios such as the noninvasive glucose determination in which the collection of a representative background spectrum is impossible.

The data preprocessing methods employed in this work (i.e., log transform, MSC, and normalization) all worked to reduce the effect of the single-beam intensity variation. Overall, MSC and normalization were observed to perform more consistently than the log transform, and are thus recommended. No significant difference between the two was observed. Digital filtering was found to be useful to reduce the model size and make the calibration models perform more consistently, but its use did not eliminate the need for a preprocessing step to remove the overall intensity variation in the single-beam spectra.

Stepwise QPLS models were never found to be statistically worse in prediction performance than the corresponding linear PLS models, and were statistically superior in several cases. The QPLS models help to account for the nonlinear relationship between single-beam spectral intensities and analyte concentrations that is described by Eq. 1. Since the degree to which this relationship deviates from linearity is a function of the magnitudes of the  $\epsilon_{k,j}bc_{i,k}$  values in Eq. 1 (i.e., small values will fall in a more linear region of the  $10^{-x}$  function), the importance of nonlinear approaches to building calibration models with single-beam spectra will vary among applications as concentrations and chemical constituents vary. Further investigation of this issue is warranted, especially with the use of more flexible nonlinear modeling methods such as artificial neural networks.

Finally, in the evaluation of the robustness of the calibration models, some degradation in performance was observed in all models when the calibration set did not span the prediction set in time. However, the models computed with single-beam spectra remained competitive with those based on absorbance spectra.

#### ACKNOWLEDGMENTS

This research was supported by the National Institutes of Health under grant DK45126. Mutua Mattu and Ndimiso Cingo are acknowledged for their assistance in collecting the spectra in the GTB\_1 data set. Neal Thathapudi is thanked for the collection of the spectra in the GTB\_2 data set. Ronald Shaffer is acknowledged for writing the original genetic algorithm software.

1. M. A. Arnold, in *Handbook of Clinical Laboratory Automation, Robotics, and Optimization*, G. R. Kost, Ed. (John Wiley and Sons, New York, 1996), Chap. 12, pp. 631–647.
2. D. M. Haaland, M. R. Robinson, G. W. Koepp, E. V. Thomas, and R. P. Eaton, *Appl. Spectrosc.* **46**, 1575 (1992).

3. R. Marbach, Th. Koschinsky, F. A. Gries, and H. M. Heise, *Appl. Spectrosc.* **47**, 875 (1993).
4. H. M. Heise, in *Biosensors in the Body. Continuous in vivo Monitoring*, D. M. Fraser, Ed. (John Wiley and Sons, New York, 1997), Chap. 3, pp. 79–116.
5. M. A. Arnold and G. W. Small, *Anal. Chem.* **62**, 1457 (1990).
6. L. A. Marquardt, M. A. Arnold, and G. W. Small, *Anal. Chem.* **65**, 3271 (1993).
7. G. W. Small, M. A. Arnold, and L. A. Marquardt, *Anal. Chem.* **65**, 3279 (1993).
8. K. H. Hazen, M. A. Arnold, and G. W. Small, *Appl. Spectrosc.* **48**, 477 (1994).
9. S. Pan, H. Chung, M. A. Arnold, and G. W. Small, *Anal. Chem.* **68**, 1124 (1996).
10. R. E. Shaffer, G. W. Small, and M. A. Arnold, *Anal. Chem.* **68**, 2663 (1996).
11. A. S. Bangalore, R. E. Shaffer, G. W. Small, and M. A. Arnold, *Anal. Chem.* **68**, 4200 (1996).
12. M. J. Mattu, G. W. Small, and M. A. Arnold, *Anal. Chem.* **69**, 4695 (1997).
13. G. Lu, X. Zhou, M. A. Arnold, and G. W. Small, *Appl. Spectrosc.* **51**, 1330 (1997).
14. N. G. Thathapudi, M.S. Thesis, Ohio University, Athens, Ohio (1998).
15. H. M. Heise and A. Bittner, *J. Mol. Struct.* **348**, 127 (1995).
16. A. Bittner, R. Marbach, and H. M. Heise, *J. Mol. Struct.* **349**, 341 (1995).
17. H. Martens and T. Næs, *Multivariate Calibration* (John Wiley and Sons, New York, 1989).
18. P. Geladi, D. McDougall, and H. Martens, *Appl. Spectrosc.* **39**, 491 (1985).
19. T. Issakson and T. Næs, *Appl. Spectrosc.* **42**, 1273 (1988).
20. T. Næs, T. Issakson, and B. Kowalski, *Anal. Chem.* **62**, 664 (1990).
21. G. Horlick, *Anal. Chem.* **44**, 943 (1972).
22. Q. Ding and G. W. Small, *Anal. Chim. Acta* **384**, 325 (1999).
23. J. Neter, M. H. Kutner, C. J. Nachtsheim, and W. Wasserman, *Applied Linear Statistical Models*, (Richard D. Irwin, Chicago, 1989), 4th ed., Chap. 7, pp. 268–269.
24. D. M. Haaland and E. V. Thomas, *Anal. Chem.* **60**, 1193 (1988).
25. D. B. Hibbert, *Chemom. Intell. Lab. Syst.* **19**, 277 (1993).
26. C. B. Lucasius and G. Kateman, *Chemom. Intell. Lab. Syst.* **19**, 1 (1993).
27. C. B. Lucasius and G. Kateman, *Chemom. Intell. Lab. Syst.* **25**, 99 (1994).